Published in final edited form as:
Mol Cell Endocrinol. 2011 February 20; 333(2): 134–142. doi:10.1016/j.mce.2010.12.021.

RANBP17 is localized to the XY body of spermatocytes and interacts with SPEM1 on the manchette of elongating spermatids

Jianqiang Bao[1,2,3,#], **Qiuxia Wu**[1,#], **Rui Song**[1], **Zhang Jie**[4], **Huili Zheng**[1], **Chen Xu**[2,3], and **Wei Yan**[1,*]

[1]Department of Physiology and Cell Biology, University of Nevada School of Medicine, Reno, Nevada, USA

[2]Department of Embryology and Histology, Shanghai Jiaotong University School of Medicine, Shanghai, China

[3]Shanghai Key Laboratory for Reproductive Medicine, Shanghai, China

[4]Department of Biochemistry, China Medical University, Shenyang, China

Abstract

We identified Ran-binding protein 17 (RANBP17) as one of the interacting partners of sperm maturation 1 (SPEM1) using yeast 2-hybrid screening and immunoprecipitation assays. Expression profiling analyses suggested that RANBP17 was preferentially expressed in the testis. Immunofluorescent confocal microscopy revealed a dynamic localization pattern of RANBP17 during spermatogenesis. In primary spermatocytes RANBP17 was mainly localized to the XY body. In the subsequent spermiogenesis, RANBP17 was first observed in the nuclei of round spermatids (steps1–7) and then confined to the manchette of elongating spermatids (steps 8–14) together with its interacting partner SPEM1. In the *Spem1*-null testes, levels of RANBP17 were significantly elevated. As a member of a large protein family involved in the nucleocytoplasmic transport, RANBP17 may have a role in sex chromosome inactivation during the meiotic phase of spermatogenesis, and also in the intramanchette transport during spermiogenesis. Interactions between RANBP17 and SPEM1, for the first time, point to a potential function of SPEM1 in the RANBP17-mediated nucleocytoplasmic transport.

Keywords

spermatogenesis; *nucleocytoplasmic transport*; *XY body*; *meiotic sex chromosome inactivation*; *manchette*; *meiosis*; *spermiogenesis*

[*]Corresponding author: Wei Yan MD, PhD *Associate Professor* Department of Physiology and Cell Biology University of Nevada School of Medicine Anderson Biomedical Science Building 105C/111 1664 North Virginia Street, MS 352 Reno, NV 89557 Tel: 775 784 7765 (Office) 775 784 4688 (Lab) Fax: 775 784 6903 wyan@medicine.nevada.edu URL: http://www.medicine.nevada.edu/physio/facyan.html.
[#]these two authors contribute equally.

INTRODUCTION

The process of producing male gametes (spermatozoa) is termed spermatogenesis, which can be divided into three phases: mitotic (spermatogonial multiplication and differentiation), meiotic (spermatocyte differentiation and meiotic cell division) and haploid (round spermatid differentiation to form elongated spermatids and eventually spermatozoa) (Clermont, 1972). Meiosis is unique to gamete (oocyte and sperm) formation, whereas haploid germ cell differentiation, also called spermiogenesis, only occurs during male germ cell development (Esponda, 1985; Wolgemuth et al., 1995). Unique processes often require unique regulatory molecules to fulfill the function, which may explain why testis-specific genes are mostly expressed in the meiotic and haploid phases of spermatogenesis (Schultz et al., 2003; Shima et al., 2004). Gene knockout studies over the past two decades have identified numerous genes/proteins that are essential for spermatogenesis (Matzuk and Lamb, 2002, 2008) and for spermiogenesis in particular (Yan, 2009).

Spem1 is one of the spermiogenesis-essential genes. *Spem1* is exclusively expressed in the testis (Zheng et al., 2007). *Spem1* mRNA can be detected in all haploid spermatids, but SPEM1 protein is mainly expressed in elongating and elongated spermatids. The delayed translation suggests a role of SPEM1 in late spermiogenesis (steps 9–16 in mouse spermiogenesis). Indeed, *Spem1* knockout male mice are infertile due to deformed spermatozoa characterized by heads bent back with cytoplasm remnants attached to the head-to-neck junction (Zheng et al., 2007). This type of “head-bent-back” sperm had been noticed in several mutant mouse lines with targeted inactivation of several genes encoding proteins involved in sperm nuclear condensation (e.g. *Prm1, Prm2, Tnp1, Tnp2, H1t2, Camk4, and Csnk2a2*) (Adham et al., 2001; Catena et al., 2006; Cho et al., 2001; Tanaka et al., 2005; Wu et al., 2000; Xu et al., 1999; Yu et al., 2000). In these mutants, however, only a portion of sperm displays this head-bent-back deformation, suggesting that abnormal nuclear events during late spermiogenesis can result in sperm deformation, and the head-bent-back phenotype may be a hallmark of abnormal late spermatid development. Interestingly, *Spem1*-null sperm uniformly display this deformation (Zheng et al., 2007). The 100% penetrance implies that SPEM1 mediates critical molecular events which are required for normal spermatid elongation and final cytoplasm removal in late spermiogenesis.

To find clues that can lead to the revelation of SPEM1 function, we performed yeast 2-hybrid screening assays to identify SPEM1-interacting partners. We found that RANBP17, encoded by a gene previously reported to be preferentially expressed in the testis (Koch et al., 2000), interacts with SPEM1. Given that most of the Ran-binding proteins are key components of the large nucleocytoplasmic importing/exporting machineries (Fried and Kutay, 2003; Steggerda and Paschal, 2002; Yudin and Fainzilber, 2009), SPEM1 may be involved in nucleocytoplasmic transport by interacting with RANBP17. We, therefore, further validated the interaction between SPEM1 and RANBP17 in the mammalian system. Furthermore, we also examined expression and localization of RANBP17 during testicular development and spermatogenesis, as well as effects of SPEM1 absence on RANBP17 levels in the testes. The dynamic expression pattern of RANBP17 during spermatogenesis suggests that RANBP17 may be involved in sex chromosome inactivation during the meiotic phase of spermatogenesis, and it may also participate in intramanchette transport during late spermiogenesis.

METHODS AND MATERIALS

Animals

Wild-type (WT) and *Spem1*-null mice on a C57Bl/6:129SvEv hybrid background were maintained in a temperature- and humidity-controlled animal facility with free access to water and food at the University of Nevada School of Medicine. Testes were collected from male mice at ages of postnatal days 7, 14, 21, 28, 35 and 42. One of the paired testes from each mouse was snap-frozen in liquid nitrogen for subsequent RNA and protein analyses. The other one was cryoprotected and cryosections were prepared for immunofluorescent staining. The animal use protocol was approved by the Institutional Animal Care and Use Committee of the University of Nevada, Reno.

Yeast 2-hybrid (Y2H) assays

Y2H screening of an adult mouse testis library using the full-length SPEM1 as bait was performed as described previously (Wang et al., 2006). Briefly, the open reading frame (ORF) of *Spem1* cDNA was subcloned into the EcoRI-Sal I sites of pGBKT7 vector as the bait construct (pGBKT7/SPEM1). Sequencing analyses were performed to verify the lack of mutation and in-frame of the ORF in the pGBKT7. The pGBKT7/Spem1 was transformed into Y187 competent yeast cells followed by mating with AH109 yeast cells transformed with an adult mouse testis cDNA library cloned into the pGADT7 vector. Clones grown on the selective medium (SD/-Leu/-Trp/-Ade/-His) were picked and the pGADT7 plasmid DNA was isolated and sequenced. Co-transformation assays were performed on non-selective (SD/-Leu/-Trp) and selective (SD/-Leu/-Ade/-His) plates by co-transforming pGADT7/Ranbp17 with an empty bait vector pGBKT7, or with pGBKT7/Spem1.

Mammalian expression constructs

The PCR fragment of the ORF of *Spem1* cDNA was subcloned into the EcoRI-KpnI sites of the pGEM-T-easy vector (Promega). Sequencing analyses confirmed that the amplified ORF of *Spem1* was mutation-free. After double digestion with EcoRI and Kpn1, the *Spem1* ORF fragment was subcloned into p3XFLAG-myc-CMV-26 expression vector (Sigma). The ORF of *Spem1* was in frame and thus the full-length SPEM1 was expected to be expressed after transfection into mammalian cell lines. We named this vector p3XFLAG-Spem1. The full-length cDNA clone for *Ranbp17* was purchased from Invitrogen (clone ID#100015361). The fragment containing full-length *Ranbp17* cDNA was subcloned into pcDNA3.1/ His-TOPO vector (Invitrogen) in frame with the deletion of the stop codon. This vector was named pcDNA3.1/ His-Ranbp17. Sequencing analyses were performed on all final expression vectors to confirm that the inserts were in frame and the sequences were mutation-free.

Cell culture and transfection

COS-7 cells (ATCC™ Cat#: CRL-1651) were cultured and transfected according to the manufacturer's instructions (PolyFect Transfection Reagent, QiaGen). Briefly, two million cells were seeded in a culture dish (100mm diameter) in Dulbecco's modified eagle medium (DMEM) (Invitrogen) supplemented with 10% fetal calf serum (FCS) (Atlanta Biologicals, Inc) and the cells usually reached 40%~80% confluence the next day. The transfection complex contains 2μg p3XFLAG-Spem1 and 2μg pcDNA3.1/ His-Ranbp17 mixed with Optimized modified eagle medium (OPT-MEM, Invitrogen) in a total volume of 300μl. An aliquot of 25μl PolyFect reagent (QiaGen) was added to the DNA mixture and mixed well by pipetting up and down several times. During the incubation at RT for 5~10min, the old culture medium was removed and the cells were washed once with 5ml Dulbecco's Phosphate-Buffered Saline (D-PBS, Invitrogen) followed by addition of 7ml complete

growth medium (containing serum and antibiotics). The transfection complex was then added directly into the culture medium followed by gently swirling to ensure uniformed distribution of the complexes. Cells were cultured at 37°C with 5% CO_2 and harvested for analyses 48h after transfection.

Co-immunoprecipitation assays

A co-immunoprecipitation kit (Roche, Cat. #: 11719386001) was used and all the procedures were carried out according to the manufacturer's protocol. Briefly, after 48h of culture, COS-7 cells transfected with p3XFLAG-Spem1 and pcDNA3.1/ His-Ranbp17 were lysed using a buffer containing 50mM Tris-HCl, pH 7.4, 150mM NaCl, 1% sodium deoxycholate, 1% NP-40 and 100mM EDTA supplemented with one tablet of protease inhibitor cocktail (Roche). Anti-His or anti-FLAG monoclonal antibodies (Sigma) and protein-G agarose slurry were added into the lysates and the incubation was performed overnight at 4°C with gentle shaking. After sequential washes with high salt and low salt washing buffers, the immunocomplex was subsequently analyzed by SDS-PAGE and standard Western blot analyses as described (Wang et al., 2006).

Northern Blot Analyses

Total RNA was isolated from heart, liver, spleen, lung, kidney, brain, stomach, small intestine, colon, testis, ovary, uterus tissues as described (Wang et al., 2006). RNA samples (15μg/lane) were fractioned in a 1.2% agarose/formaldehyde gel and transferred to nylon membrane (Hybond –XL, Amersham Biosciences) followed by UV cross-linking (Spectrolinker XL-1500, Spectronics Corp.). A 324bp-long probe corresponding to exons 2–4 of *Ranbp17* was amplified from mouse testicular cDNAs using PCR with primers (forward: 5′-TCTGGATGACACTGCTACCG-3′; reverse: 5′-GCATCATGCTCATCTGTGCT-3′). The probe was labeled with [α-^{32}P]-dCTP using a Rediprime II Labeling Kit (Amersham). Hybridization, washing, and autoradiography were performed as described (Jin et al., 2005). Gel images of the 28S and 18S bands were used as loading and mRNA quality controls.

Semi-quantitative and real-time PCR

Spermatogenic cell populations were purified as described (Song et al., 2009). RNA isolation and cDNA synthesis were performed as described (Song et al., 2009). Primers used are as follows: *Spem1*: 5'-GCTGCTCTTGGGTCTTATCG-3' (forward), 5'-TGGACTTTGGGGTAGGTCTG-3' (reverse); *Ranbp17*: 5'-GGCTGAGAAAGCACTCTTGG-3' (forward), 5'-GTTGGGACGCCACATAATTC-3'(reverse); *Gapdh*: 5'-GGCATTGCTCTCAATGACAA-3' (forward), 5'-TGTGAGGGAGATGCTCAGTG-3' (reverse). For semi-quantitative PCRs, amplification was performed at 25–28 cycles, which were tested to be in the exponential range. For real-time PCRs, a SYBR green-based method was used as described (Song et al., 2009). Mouse reference genes *Hprt* and *Gapdh* were used as the loading/internal control (Wang et al., 2006) (Song et al., 2009).

Immunofluorescent staining and confocal microscopy

Testes of adult mice were dissected and fixed in 4% paraformaldehyde for 3h at 4°C. The fixed testes were then cryoprotected in serial sucrose solutions with increasing concentrations by mixing 5% and 20% sucrose in ratios of 2:1, 1:1 and 1:2, respectively. The testis samples were incubated for 1/2 hour in each of the sucrose mixtures at room temperature followed by a final incubation in 20% sucrose at 4°C overnight. The testes were then embedded into sucrose: OCT of 1:1. Cryosections of 10-μm thickness were prepared for immunofluorescent staining. The slides were blocked in normal goat and fetal bovine

sera at room temperature for 1hr in a humidity box. An affinity-purified, rabbit polyclonal antibody raised against the full-length human RNABP17 (Abcam, Cat#ab15017, diluted at 1:200) was added onto the sections and the slides were placed into a humidity box for overnight incubation at 4°C. The slides were washed with 1XPBS for 3 times prior to incubation with an AlexaFLuo488-conjugated goat-anti-rabbit secondary antibody (Molecular Probes, at a dilution of 1:500) for 1hr. After three times of washing with 1XPBS, coverslips were applied using aqueous mounting medium containing propidium iodide. Imaging analyses was conducted using a confocal microscope (Carl Zeiss, LSM510).

Dissection of stage-defined seminiferous tubule segments and squash preparation were performed as described with a minor modification (Yan et al., 2000). After fixation with 4% freshly-prepared paraformaldehyde at RT for 15min, slides with the squashed seminiferous tubules were permeabilized by boiling 3 times (5min each) in 1 × Citrate buffer (pH6.0) using a microwave oven. Washed with 1XPBS for 3 times (5min each), the slides were then blocked with 100μl blocking buffer (30μl fetal bovine serum + 30μl normal goat serum + 960μl 0.1M PBS) at RT for 1hr. Primary antibody incubation was performed at 4°C overnight. The rabbit-anti-RANBP17 polyclonal antibody and a mouse anti-β-Tubulin monoclonal antibody (Developmental Studies Hybridoma Bank, E7-c, diluted at 1:500) were used for the co-localization assays. Rabbit anti-SPEM1 polyclonal antibody was prepared as described (Zheng et al., 2007) and used at a dilution of 1:1,000. The next day, the slides were moved to RT for at least 30min before being washed 3 times with 1XPBS (10min per wash). The slides were then incubated with the fluorescence-conjugated, species-specific secondary antibodies (Molecular Probes) at room temperature for 1hr with gently shaking, followed by washing with 1XPBS 3 times (10min per wash). Finally the slides were counterstained with 4',6-diamidino-2-phenylindole (DAPI) or propidium iodide (PI) for immunofluorescent assay using a confocal microscope (Olympus, FV1000).

Meiotic chromosome Spread

Meiotic chromosome spreads were prepared using the drying-down technique (Namekawa et al., 2007; Peters et al., 1997). In brief, seminiferous tubules were gently teased apart in PBS, and some tubules were transferred to hypotonic extraction buffer [30mM Tris, 50mM sucrose, 17mM trisodium citrate dihydrate, 5mM ethylenediaminetetraacetic acid (EDTA), 0.5mM dithiothreitol (DTT), and 0.5mM phenylmethylsulfonyl fluoride (PMSF)] and incubated at room temperature for 30–60min. Seminiferous tubules (~1 cm in length) were torn to pieces in 20μl of 100mM sucrose. Then the volume was increased to 40μl with 100mM sucrose. Half of the cell suspension was dispersed onto slides that had just been incubated in a paraformaldehyde solution (1%PFA, 0.05% Triton X-100, 0.02% SDS, pH 9.2). The slides were then incubated overnight in a humid chamber. Slides were washed twice in 0.4% Photo Flo (Kodak) and dried at room temperature. The spreads were rehydrated in PBS. Immunostaining was performed as described above. For co-localization assays, a rabbit anti-RANBP17 polyclonal antibody (diluted at 1:100) and mouse anti-γH2Ax (Abcam, ab2255 diluted at 1:800) or mouse anti-SCP3 (a component of axial elements (Schalk et al., 1998); kindly provided by Dr. Paula Cohen and used at a dilution 1:800) antibodies were used. Images were captured using a confocal microscope (Olympus, FV1000).

Western blot analyses

Western blot analyses were performed as described previously (Wang et al., 2006). Briefly, total protein was isolated from mouse testes or cultured COS-7 cells. Protein lysates (100μg/lane) were fractionated on 10% Tris-HCl polyacrylamide gels through electrophoresis and transferred onto nitrocellulose membranes (Bio-Rad). The membrane was then blocked with 5% non-fat milk. Primary antibody incubation was conducted at RT for 1hr. After three

washes with PBST (1XPBS containing 0.1% Tween20), membranes were incubated with a secondary antibody conjugated with horseradish peroxidase (1:1,000, Amersham) for 1 hr, followed by washing. An enhanced chemiluminescence detection system (Amersham) was used for detection of specific proteins.

RESULTS

Identification of RANBP17 as a SPEM1-interacting protein

We used SPEM1 as bait and screened an adult mouse testis library using the Y2H system. Y2H screening assays yielded 98 clones, 37 of which contained cDNA sequences for *Ranbp17*, a gene encoding Ran-binding protein 17 (RANBP17). Co-transformation assays were performed on non-selective (SD/-Leu/-Trp) and selective (SD/-Leu/-Trp/-Ade/-His) medium plates by co-transforming pGADT7/Ranbp17 with the empty bait vector pGBKT7, or with pGBKT7/Spem1 (Fig. 1A). The non-selective plates showed yeast cell growth among all the co-transformations (Fig. 1A, left panel), indicating that the yeast cells were viable and the plasmid constructs were non-toxic. The selective plates only showed yeast cell growth in the co-transformations between pGBKT7/Spem1 and pGADT7/Ranbp17 (Fig. 1A, right panel). These results confirmed interactions between SPEM1 and RANBP17 in the yeast cells.

To further examine interactions between SPEM1 and RANBP17 in the mammalian system, we transfected plasmids expressing FLAG-tagged SPEM1 and/or His-tagged RANBP17 into COS-7 cells. Expression of the two proteins with correct sizes was verified using Western blot analyses (Fig. 1B, upper panels). In the FLAG pull-down products, His-tagged RANBP17 was detected (Fig. 1B, lower panel), demonstrating that SPEM1 and RANBP17 interact not only in the yeast cells, but also in mammalian cells.

We further examined levels of RANBP17 in *Spem1* knockout testes using Western blot analyses (Fig. 1C). At light microscopic levels, the adult *Spem1*-null testes are indistinguishable from testes of the adult WT or $Spem1^{+/-}$ mice (Zheng et al., 2007). Therefore, the cellular composition among testes of these three genotypes is comparable and Western blot-based protein quantification could reveal differences in RANBP17 levels. In *Spem1*-null testes, RANBP17 levels were almost three times higher than those in the WT or $Spem1^{+/-}$ testes.

Semi-quantitative (Fig.1D, left panel) and real-time (Fig.1D, right panel) PCRs were performed to examine levels of *Ranbp17* mRNA in wild-type (WT) and *Spem1*-null testes. Both quantitative PCR analyses revealed no significant changes in *Rnabp17* mRNA levels in WT and *Spem1*-null testes, suggesting the elevated levels of RNABP17 protein is achieved through post-transcriptional regulation. *Rnabp17* mRNA has been shown to be ribonuclear particle (RNP)-bound (translationally suppressed status) at P17 testes (pachytene spermatocytes are dominant in number and spermatids are absent) and become more polyribosome-associated (translationally active state) in adult testes (Iguchi et al., 2006), suggesting *Ranbp17* transcripts are subject to post-transcriptional regulation. Given that *Ranbp17* mRNA levels remain unchanged in the absence of *Spem1*, the elevated levels of RANBP17 protein are most likely achieved through enhanced translation and/or reduced turnover rate of *Rnabp17* transcript. The upregulation of RANBP17 in *Spem1*-null testes may represent a compensatory effect due to the loss of SPEM1. This finding further support interactions between SPEM1 and RANBP17 *in vivo*.

RANBP17belongs to β-importin family and is highly conserved among mammalian species

Mouse *Ranbp17* gene consists of 28 exons expanding ~301 kb on the minus strand of chromosome 11 (Supplemental Fig. 1A). The full-length RANBP17 protein contains 1088

a.a. and there are two known functional domains in its N-terminus: armadillo (ARD)-type fold and importin-β domain (Supplemental Fig. 1A). The ARD-type fold is a multi-helical fold comprised of two curved layers of α-helices arranged in a regular right-handed superhelix (Groves and Barford, 1999; Striegl et al., 2009). These superhelical structures present an extensive solvent-accessible surface that is believed to bind large substrates such as proteins and nucleic acids (Groves and Barford, 1999). Many proteins involved in nucleocytoplasmic transport, e.g. importins and exportins, contain this domain (Okada et al., 2008; Weis, 1998). Importin-β domain has been shown to be able to bind Ran GTPase, which controls the unidirectional transport of cargo proteins during the exchange of macromolecules between the nucleus and cytoplasm (Harel and Forbes, 2004). Therefore, importin-β domain-containing proteins are also members of a large Ran-binding protein family (Sorokin et al., 2007). The phylogenetic analyses revealed that RANBP16 and RANBNP17 are the closest paralogs among 16 Ran-binding proteins collected in the databases (Supplemental Fig. 1B). Multiple alignment analyses of RANBP17 orthologs showed a high degree of conservation with amino acid similarity >92% among all 6 mammalian species analyzed (Supplemental Figs. 1C and 2). Humans and mice share 94% sequence similarity in RANBP17 (Supplemental Fig. 1C), suggesting a conserved physiological role of this protein.

Expression profiles of Ranbp17 mRNA and protein

We next examined the expression profile of *Ranbp17* mRNA and protein. Northern blot analyses detected *Ranbp17* mRNA predominantly in the testis (Fig. 2A). This result is consistent with a previous study showing the detection of *Ranbp17* mRNA exclusively in the testis (Koch et al., 2000). To further corroborate these data, we also examined two major online gene expression databases including the Gene Expression Profile in silico (GeneHub-GEPIS) (http://www.cgl.ucsf.edu/Research/genentech/genehub-gepis/index.html) and the NCBI-based gene expression omnibus (GEO) profiles (http://www.ncbi.nlm.nih.gov/sites/geo/). The GeneHub-GEPIS is a bioinformatics tool for inferring gene expression patterns in a large panel of normal and cancer tissues based on human and mouse EST sequence abundance (Zhang et al., 2007). The GEO profiles are based upon microarray analyses. In both databases, both mouse and human *Ranbp17* mRNAs displays the highest expression levels in the testis. Lower levels are also present in other organs including adrenal gland, lung and retina. Therefore, *Ranbp17* is a gene preferentially expressed in the testis. (In GEO profile the GPL546 set is for *Ranbp17* expression in multiple tissues).

In developing testes, *Ranbp17* mRNA was first detected in postnatal day 14 (P14) testes and its mRNA levels increased thereafter and peaked at P28 (Fig. 2B). This result is similar to multiple sets of microarray data on *Ranbp17* mRNA expression in developing testes in mice (the GPL1262 set in GEO Profile). The expression pattern of RANBP17 protein in developing testes (Fig. 2C) was similar to that of *Ranbp17* mRNA (Fig. 2B). RANBP17 was first detected in P14 testes and levels peaked at P28 and P35 (Fig. 2C). The onset of *Ranbp17* mRNA and protein expression between P7 and P14 coincides with the first appearance of early spermatocytes in developing testes, suggesting *Ranbp17* mRNA and protein are first expressed in meiotic germ cells. Both *Ranbp17* mRNA and protein levels peaked between P28 and P35, coinciding with spermatid elongation and condensation, suggesting a potential role of RANBP17 in spermiogenesis.

Using a semi-quantitative PCR method (Jin et al., 2005; Song et al., 2009), we also investigated levels of *Ranbp17* mRNAs in purified testicular cell populations (Fig. 2D). *Ranbp17* mRNA levels were the highest in pachytene spermatocytes and round spermatids. Medium levels were detected in leptotene, zygotene, and early pachytene spermatocytes. Low to undetectable levels were observed in Sertoli cells, type A and type B spermatogonia,

as well as in preleptotene spermatocytes. In summary, these expression data suggest that *Ranbp17* mRNA and protein are expressed in meiotic spermatocytes and haploid spermatids, and their levels peak in spermatids during late spermiogenesis.

Dynamic localization of RANBP17 during spermatogenesis

We next examined the localization of RANBP17 using immunofluorescent confocal microscopy. The anti-RANBP17 polyclonal antibody was tested to be specific by neutralization experiments, in which the antibody that was neutralized with an excessive amount of RANBP17-expressing COS-7 cell lysates in Western blot analyses and immunohistochemistry (data not shown). In addition, single bands corresponding to the expected size of RANBP17 (125kDa) in Western blots also suggested the high specificity of this antibody (Fig. 2C). RANBP17 appears to be localized mainly to the nuclei of spermatocytes and round spermatids (Fig. 3). Lower levels of RANBP17 immunoreactivity were first detected between leptotene to zygotene transition and the levels did not increase until early pachytene spermatocytes (Fig. 3). In pachytene spermatocytes, RANBP17 immunoreactivity appeared to be more intense in a sub/peri-nuclear domain resembling the sex body (top three panels in Fig. 3). In other areas of the nuclei of pachytene spermatocytes, RNABP17 immunoreactivity seemed to be increasing from early to late pachytene stages (note more intense staining in the nuclei of Stage VIII pachytene spermatocytes than in those of Stage VII pachytene spermatocytes in Fig. 3). RANBP17 immunoreactivity shifted completely to the nuclei in meiotically dividing spermatocytes and appeared much stronger than in the main areas of the nuclei of pachytene spermatocytes (areas excluding the XY body). In spermatids, RANBP17 was first detected in the nuclei of round spermatids (steps 1–7) with levels comparable to those in the main areas of the nuclei of pachytene spermatocytes. From step 8 onward, RANBP17 appeared to be mainly localized to a structure resembling the manchette in elongating spermatids (steps 8–14). In elongated spermatids (steps15–16), RANBP17 immunoreactivity gradually diminished to undetectable levels.

High-power immunofluorescent confocal images further confirmed that in spermatocytes, RANBP17 was predominantly localized to a structure resembling the XY body in pachytene and diplotene spermatocytes and in the nuclei of meiotically dividing spermatocytes (arrowheads in Supplemental Fig.3, upper panels). During late spermiogenesis, RANBP17 was localized to structures reminiscent of the manchette of elongating spermatids (arrows in Supplemental Fig.3).

RANBP17 is highly concentrated in the XY body and is associated with chromosomes

To confirm that RANBP17 was indeed localized to the XY body, we performed co-localization studies using anti- γH2Ax antibody and testis cryosections (Supplemental Fig. 4). γH2Ax has been used as a marker for the XY body (Sciurano et al., 2007; Song et al., 2009) because it is associated only with sex chromosomes in the XY body of pachytene and diplotene spermatocytes (Hamer et al., 2003; Sciurano et al., 2007). In pachytene spermatocytes, RANBP17 and γH2Ax both were colocalized to the XY body (arrows in Supplemental Fig. 4). γH2Ax was also detected in the nuclei of leptotene and zygotene spermatocytes, but RANBP17 was absent in these cells. RANBP17 is detected in the perinuclear region resembling the manchette of elongating spermatids, whereas γH2Ax was not detected in these cells (arrowheads in Supplemental Fig. 4).

To test whether RANBP17 is associated with chromatin, we prepared meiotic chromatin spreads followed by immunofluorescent detection of γH2Ax, SCP3 (a component of the axial elements in synaptonemal complexes) and RANBP17 (Fig. 4). In pachytene spermatocyte chromosome spreads, γH2Ax immunoreactivity was confined to the XY body,

whereas RNABP17 immunoreactivity was predominantly co-localized with γH2Ax to the XY body. Interestingly, RANBP17 immunoreactivity was also detectable in the autosomal domain (Fig. 4, upper panels). The synaptonemal complexes were clearly stained by the anti-SCP3 antibody in meiotic chromosome spreads (Fig. 4, lower panels). RANBP17 immunoreactivity was much stronger in the sex body than in the autosomal domain. Together, these data demonstrate that RANBP17 is generally associated with all chromosomes, but predominantly associated sex chromosomes and thus mainly localized to the XY body in pachytene spermatocytes.

The subcellular localization pattern of RANBP17 during mouse spermatogenesis is schematically summarized in Supplemental Fig.3 (lower panel).

RANBP17 and SPEM1 are co-localized to the manchette of elongating spermatids

Using squash preparation and immunofluorescent confocal microscopy, we further examined the localization of RANBP17 and SPEM1 in developing spermatids (Figs. 5 and 6). The manchette is a transient apparatus which starts to be formed in step 8 spermatids (coinciding with the onset of elongation) and disappears in step 13/14 spermatids (by the end of elongation and condensation). The manchette is enriched of microtubules and F actin. β-Tubulin has therefore been used as a marker for the manchette (Mochida et al., 1998;Rivkin et al., 1997;Yoshida et al., 1994). The manchette is believed to be critical in shaping the sperm head, in the transport of vesicles and macromolecules to the centrosome and the developing spermatid tail as well as in nuclear-cytoplasmic transport (Kierszenbaum, 2002;Kierszenbaum and Tres, 2004). RANBP17 was indeed co-localized with β-Tubulin to the manchette of elongating spermatids (Fig. 5). Similarly, SPEM1 was also localized to the manchette (Fig. 6). Since the RANBP17 and SPEM1 antibodies were all raised in rabbits, we could not perform RANBP17 and SPEM1 co-localization assays. However, the common localization of these two proteins to the manchette is consistent with our Y2H and pull-down assays (Fig. 1), demonstrating these two proteins directly interact with each other on the manchette during the elongation and condensation steps of spermiogenesis.

Given that RANBP17 levels were significantly up-regulated in *Spem1*-null testes (Fig. 1C), we further investigated the localization of RANBP17 in spermatids of *Spem1*-null testes (Supplemental Fig. 5). We have previously shown that the “head-bent-back” phenotype starts during spermiogenesis within the testis rather than during the epididymal transition (Zheng et al., 2007). Although monolayer of spermiogenic cells was formed in the squash preparations (Supplemental Fig. 5), the morphology of the manchette outlined by β-Tubulin staining was a bit different from that seen in WT elongating spermatids (Figs. 5 and 6). *Spem1*-null elongating spermatids displayed patchy and uneven distribution of β-Tubulin signals over the manchette, comparing to the homogeneously smooth-looking β-Tubulin or SPEM1 staining in the manchette of WT elongating spermatids. Nevertheless, both RANBP17 and β-Tubulin remained to be expressed and their expression was confined to the manchette (Supplemental Fig. 5).

DISCUSSION

Our recent gene knockout study reveals that SPEM1 is essential for normal sperm production and thus for male fertility (Zheng et al., 2007). However, the molecular mechanism underlying the unique phenotype characterized by the “head-bent-back” deformation of spermatozoa (with 100% penetrance) remains unknown. Since there is no known conserved functional domain in SPEM1 protein, it is difficult to predict its molecular action. In this study we discovered that SPEM1 interacts with RANBP17, and this interaction most likely takes place on the manchette of elongating spermatids.

RANBP17 belongs to a large Ran-binding protein superfamily (Sorokin et al., 2007). Members of this protein family all contain the importin-β domain, through which Ran-GTP/GDP binds (Harel and Forbes, 2004; Okada et al., 2008). In addition, they also directly bind their cargo proteins (Sorokin et al., 2007). Depending upon the status of Ran, either Ran-GTP or Ran-GDP, Ran-binding proteins function as exportins or importins, respectively. Unlike most of members of the RAN-binding protein family, RANBP17 is preferentially expressed in the testis, as demonstrated by a previous study (Koch et al., 2000) and our data herein. The testis-preferential expression suggests that RANBP17 has a role preferentially assigned to the testis. The fact that RANBP17 is predominantly expressed in the XY body of pachytene spermatocytes and the manchette of elongating spermatids suggests that this protein may have a role in two important spermatogenic events: meiotic sex chromosome inactivation (MSCI) and late spermiogenesis (spermatid elongation and nuclear condensation).

During the meiotic phase of spermatogenesis, sex chromosomes (X and Y) in spermatocytes are not only physically segregated from other paired autosomes and are confined to a peripheral nuclear subdomain called the XY body (or the sex body) (Handel, 2004; Hoyer-Fender, 2003), but also transcriptionally silenced through a yet-to-be-defined mechanism (Khalil and Wahlestedt, 2008; Turner, 2007). This process has been termed meiotic sex chromosome inactivation (MSCI). It is conceivable that communication between XY body and the other nuclear domains or between nucleus and cytoplasm must be constant and critical during MSCI. This communication is likely achieved through proteins or RNAs that are shuttling between these functional domains. Given that RANBP17 is a potential Ran-binding cargo protein, it may be involved in these events based upon its localization patterns in spermatocytes. Unlike the phosphorylated form of H2Ax (γH2Ax) which is exclusively associated with the sex chromosomes in the XY body during MSCI, RANBP17 appears to be more concentrated in the XY body, but remains associated with autosomes. This suggests that its function is not solely limited to MSCI. It is more likely that RANBP17 mediates communication between the transcriptionally silenced sex chromosomes and active autosomes during MSCI. Given that the resolution of our immunofluorescent microscopic analyses did not allow the detection of much lower levels of RNABP17 in the cytoplasm, a potential role of RANBP17 in nucleus-cytoplasm transport cannot be excluded. However, the significantly elevated levels of RANBP17 in the XY body compared to other autosomal domains in pachytene spermatocytes suggest that this potential Ran-cargo protein is involved in MSCI. Further studies are needed to elucidate its role as either an importin or an exportin, and the cargo proteins that it carries during MSCI. Since SPEM1 is not expressed in meiotic spermatocytes (Zheng et al., 2007), the role of RANBP17 in meiosis is independent of SPEM1.

The manchette is a microtubular structure surrounding the elongating and condensing nuclei of steps 8–14 spermatids in mice (Kierszenbaum and Tres, 2004). Given its microtubule-enriched nature, it has been suggested that the manchette may play a role in shaping the head of sperm (Kierszenbaum, 2002a; Kierszenbaum and Tres, 2004). Another potential function of the manchette has been proposed as a transporting apparatus based upon the fact that many motor proteins (i.e. kinesins and dyneins), or nuclear-cytoplasmic shuttle proteins (i.e. Ran-GTP) are localized to the manchette (Kierszenbaum, 2002a). Localization of RANBP17 to the manchette supports the role of the manchette as a platform of nucleus-cytoplasm transport (Kierszenbaum, 2002; Kierszenbaum et al., 2007; Kierszenbaum and Tres, 2004). Co-existence of RANBP17 and Ran-GTP/GDP on the manchette suggests that active trafficking between the elongating and condensing nucleus and cytoplasm of spermatids is achieved at least partially through the intramanchette transport system. Interactions between RANBP17 and SPEM1 and their co-localization to the manchette suggest two possible roles: one is that SPEM1 may be the cargo protein for RANBP17. However, this is not

supported by the fact that 1) SPEM1 expression is confined to the cytoplasm and 2) *Spem1*-null sperm nuclei are competent to produce normal pups through intracytoplasmic sperm injection (ICSI) (Zheng et al., 2007). The other possibility is that SPEM1 may function as a scaffold protein linking RANBP17's cargo proteins to other processing machineries in the cytoplasm of elongating spermatids. This hypothesis is supported by our recent discovery that SPEM1 in fact interacts with UBQLN1, a polyubiquitin chain-interacting protein involved in the ubiquitin-proteasome system (Bao et al., 2010).

Spem1-null sperm display the “head-bent-back” deformation with 100% penetrance. Except for bending at the junction of the head and the neck, the structure of sperm tails appears to be normal as demonstrated by electron microscopic (EM) studies, and both structure and function of the *Spem1*-null sperm head are also normal based upon EM studies and ICSI experiments (Zheng et al., 2007). These facts imply that SPEM1-RANBP17-mediated intramanchette transport is involved in neither transporting structural proteins to the developing centrosome and tail, nor importing nuclear condensation proteins (e.g. protamine) to the nucleus. It would be interesting to further investigate what cargo proteins that RANBP17 carries and how interactions between SPEM1 and RANBP17 affect the fate of the cargo proteins.

In summary, we have identified that SPEM1 is localized to the manchette of elongating spermatids, on which it interacts with RANBP17, a potential Ran-dependent importin or exportin that can carry cargo proteins in and out of the nucleus and thus is involved in the intramanchette transport during spermiogenesis. In addition, RANBP17 is highly concentrated in the XY body in spermatocytes undergoing MSCI, and it thus may participate in MSCI during the meiotic phase of spermatogenesis

Supplementary Material

Refer to Web version on PubMed Central for supplementary material.

Acknowledgments

Dr. John R. McCarrey is acknowledged for providing us with the purified testicular cells. This work is supported by a grant from the NIH (HD050281 and HD060858) and by funds from the University of Nevada, Reno, to W.Y.. C.X. was supported by a grant for the Shanghai Leading Academic Discipline Project (Project#: S30201) and fund from the Science and Technology Commission of Shanghai Municipality (10DZ2270600). J.B. was supported by a scholarship from the Chinese Scholarship Council.

REFENCES

Adham IM, Nayernia K, Burkhardt-Gottges E, Topaloglu O, Dixkens C, Holstein AF, Engel W. Teratozoospermia in mice lacking the transition protein 2 (Tnp2). Mol Hum Reprod 2001;7:513–520. [PubMed: 11385107]

Bao J, Zhang J, Zheng H, Xu C, Yan W. UBQLN1 interacts with SPEM1 and participates in spermiogenesis. Mol Cell Endocrinol 2010;327:89–97. [PubMed: 20558241]

Catena R, Ronfani L, Sassone-Corsi P, Davidson I. Changes in intranuclear chromatin architecture induce bipolar nuclear localization of histone variant H1T2 in male haploid spermatids. Dev Biol 2006;296:231–238. [PubMed: 16765935]

Cho C, Willis WD, Goulding EH, Jung-Ha H, Choi YC, Hecht NB, Eddy EM. Haploinsufficiency of protamine-1 or -2 causes infertility in mice. Nat Genet 2001;28:82–86. [PubMed: 11326282]

Clermont Y. Kinetics of spermatogenesis in mammals: seminiferous epithelium cycle and spermatogonial renewal. Physiol Rev 1972;52:198–236. [PubMed: 4621362]

Esponda P. Spermiogenesis and spermatozoa in mammals. Revis Biol Celular 1985;6:1–99. [PubMed: 3916660]

Fried H, Kutay U. Nucleocytoplasmic transport: taking an inventory. Cell Mol Life Sci 2003;60:1659–1688. [PubMed: 14504656]

Groves MR, Barford D. Topological characteristics of helical repeat proteins. Curr Opin Struct Biol 1999;9:383–389. [PubMed: 10361086]

Hamer G, Roepers-Gajadien HL, van Duyn-Goedhart A, Gademan IS, Kal HB, van Buul PP, de Rooij DG. DNA double-strand breaks and gamma-H2AX signaling in the testis. Biol Reprod 2003;68:628–634. [PubMed: 12533428]

Harel A, Forbes DJ. Importin beta: conducting a much larger cellular symphony. Mol Cell 2004;16:319–330. [PubMed: 15525506]

Iguchi N, Tobias JW, Hecht NB. Expression profiling reveals meiotic male germ cell mRNAs that are translationally up- and down-regulated. Proc Natl Acad Sci U S A 2006;103:7712–7717. [PubMed: 16682651]

Jin JL, O'Doherty AM, Wang S, Zheng H, Sanders KM, Yan W. Catsper3 and catsper4 encode two cation channel-like proteins exclusively expressed in the testis. Biol Reprod 2005;73:1235–1242. [PubMed: 16107607]

Kierszenbaum AL. Intramanchette transport (IMT): managing the making of the spermatid head, centrosome, and tail. Mol Reprod Dev 2002;63:1–4. [PubMed: 12211054]

Kierszenbaum AL, Rivkin E, Tres LL. Molecular biology of sperm head shaping. Soc Reprod Fertil Suppl 2007;65:33–43. [PubMed: 17644953]

Kierszenbaum AL, Tres LL. The acrosome-acroplaxome-manchette complex and the shaping of the spermatid head. Arch Histol Cytol 2004;67:271–284. [PubMed: 15700535]

Koch P, Bohlmann I, Schafer M, Hansen-Hagge TE, Kiyoi H, Wilda M, Hameister H, Bartram CR, Janssen JW. Identification of a novel putative Ran-binding protein and its close homologue. Biochem Biophys Res Commun 2000;278:241–249. [PubMed: 11071879]

Matzuk MM, Lamb DJ. Genetic dissection of mammalian fertility pathways. Nat Cell Biol 2002;4(Suppl):s41–49. [PubMed: 12479614]

Matzuk MM, Lamb DJ. The biology of infertility: research advances and clinical challenges. Nat Med 2008;14:1197–1213. [PubMed: 18989307]

Mochida K, Tres LL, Kierszenbaum AL. Isolation of the rat spermatid manchette and its perinuclear ring. Dev Biol 1998;200:46–56. [PubMed: 9698455]

Namekawa SH, VandeBerg JL, McCarrey JR, Lee JT. Sex chromosome silencing in the marsupial male germ line. Proc Natl Acad Sci U S A 2007;104:9730–9735. [PubMed: 17535928]

Okada N, Ishigami Y, Suzuki T, Kaneko A, Yasui K, Fukutomi R, Isemura M. Importins and exportins in cellular differentiation. J Cell Mol Med 2008;12:1863–1871. [PubMed: 18657223]

Peters AH, Plug AW, van Vugt MJ, de Boer P. A drying-down technique for the spreading of mammalian meiocytes from the male and female germline. Chromosome Res 1997;5:66–68. [PubMed: 9088645]

Rivkin E, Cullinan EB, Tres LL, Kierszenbaum AL. A protein associated with the manchette during rat spermiogenesis is encoded by a gene of the TBP-1-like subfamily with highly conserved ATPase and protease domains. Mol Reprod Dev 1997;48:77–89. [PubMed: 9266764]

Schalk JA, Dietrich AJ, Vink AC, Offenberg HH, van Aalderen M, Heyting C. Localization of SCP2 and SCP3 protein molecules within synaptonemal complexes of the rat. Chromosoma 1998;107:540–548. [PubMed: 9933407]

Schultz N, Hamra FK, Garbers DL. A multitude of genes expressed solely in meiotic or postmeiotic spermatogenic cells offers a myriad of contraceptive targets. Proc Natl Acad Sci U S A 2003;100:12201–12206. [PubMed: 14526100]

Sciurano R, Rahn M, Rey-Valzacchi G, Solari AJ. The asynaptic chromatin in spermatocytes of translocation carriers contains the histone variant gamma-H2AX and associates with the XY body. Hum Reprod 2007;22:142–150. [PubMed: 16920723]

Shima JE, McLean DJ, McCarrey JR, Griswold MD. The murine testicular transcriptome: characterizing gene expression in the testis during the progression of spermatogenesis. Biol Reprod 2004;71:319–330. [PubMed: 15028632]

Song R, Ro S, Michaels JD, Park C, McCarrey JR, Yan W. Many X-linked microRNAs escape meiotic sex chromosome inactivation. Nat Genet 2009;41:488–493. [PubMed: 19305411]

Sorokin AV, Kim ER, Ovchinnikov LP. Nucleocytoplasmic transport of proteins. Biochemistry (Mosc) 2007;72:1439–1457. [PubMed: 18282135]

Steggerda SM, Paschal BM. Regulation of nuclear import and export by the GTPase Ran. Int Rev Cytol 2002;217:41–91. [PubMed: 12019565]

Striegl H, Roske Y, Kummel D, Heinemann U. Unusual armadillo fold in the human general vesicular transport factor p115. PLoS One 2009;4:e4656. [PubMed: 19247479]

Tanaka H, Iguchi N, Isotani A, Kitamura K, Toyama Y, Matsuoka Y, Onishi M, Masai K, Maekawa M, Toshimori K, et al. HANP1/H1T2, a novel histone H1-like protein involved in nuclear formation and sperm fertility. Mol Cell Biol 2005;25:7107–7119. [PubMed: 16055721]

Wang S, Zheng H, Esaki Y, Kelly F, Yan W. Cullin3 is a KLHL10-interacting protein preferentially expressed during late spermiogenesis. Biol Reprod 2006;74:102–108. [PubMed: 16162871]

Weis K. Importins and exportins: how to get in and out of the nucleus. Trends Biochem Sci 1998;23:185–189. [PubMed: 9612083]

Wolgemuth DJ, Rhee K, Wu S, Ravnik SE. Genetic control of mitosis, meiosis and cellular differentiation during mammalian spermatogenesis. Reprod Fertil Dev 1995;7:669–683. [PubMed: 8711204]

Wu JY, Ribar TJ, Cummings DE, Burton KA, McKnight GS, Means AR. Spermiogenesis and exchange of basic nuclear proteins are impaired in male germ cells lacking Camk4. Nat Genet 2000;25:448–452. [PubMed: 10932193]

Xu X, Toselli PA, Russell LD, Seldin DC. Globozoospermia in mice lacking the casein kinase II alpha' catalytic subunit. Nat Genet 1999;23:118–121. [PubMed: 10471512]

Yan W. Male infertility caused by spermiogenic defects: lessons from gene knockouts. Mol Cell Endocrinol 2009;306:24–32. [PubMed: 19481682]

Yan W, Suominen J, Toppari J. Stem cell factor protects germ cells from apoptosis in vitro. J Cell Sci 2000;113(Pt 1):161–168. [PubMed: 10591635]

Yoshida T, Ioshii SO, Imanaka-Yoshida K, Izutsu K. Association of cytoplasmic dynein with manchette microtubules and spermatid nuclear envelope during spermiogenesis in rats. J Cell Sci 1994;107(Pt 3):625–633. [PubMed: 8006076]

Yu YE, Zhang Y, Unni E, Shirley CR, Deng JM, Russell LD, Weil MM, Behringer RR, Meistrich ML. Abnormal spermatogenesis and reduced fertility in transition nuclear protein 1-deficient mice. Proc Natl Acad Sci U S A 2000;97:4683–4688. [PubMed: 10781074]

Yudin D, Fainzilber M. Ran on tracks--cytoplasmic roles for a nuclear regulator. J Cell Sci 2009;122:587–593. [PubMed: 19225125]

Zhang Y, Luoh SM, Hon LS, Baertsch R, Wood WI, Zhang Z. GeneHub-GEPIS: digital expression profiling for normal and cancer tissues based on an integrated gene database. Nucleic Acids Res 2007;35:W152–158. [PubMed: 17545196]

Zheng H, Stratton CJ, Morozumi K, Jin J, Yanagimachi R, Yan W. Lack of Spem1 causes aberrant cytoplasm removal, sperm deformation, and male infertility. Proc Natl Acad Sci U S A 2007;104:6852–6857. [PubMed: 17426145]

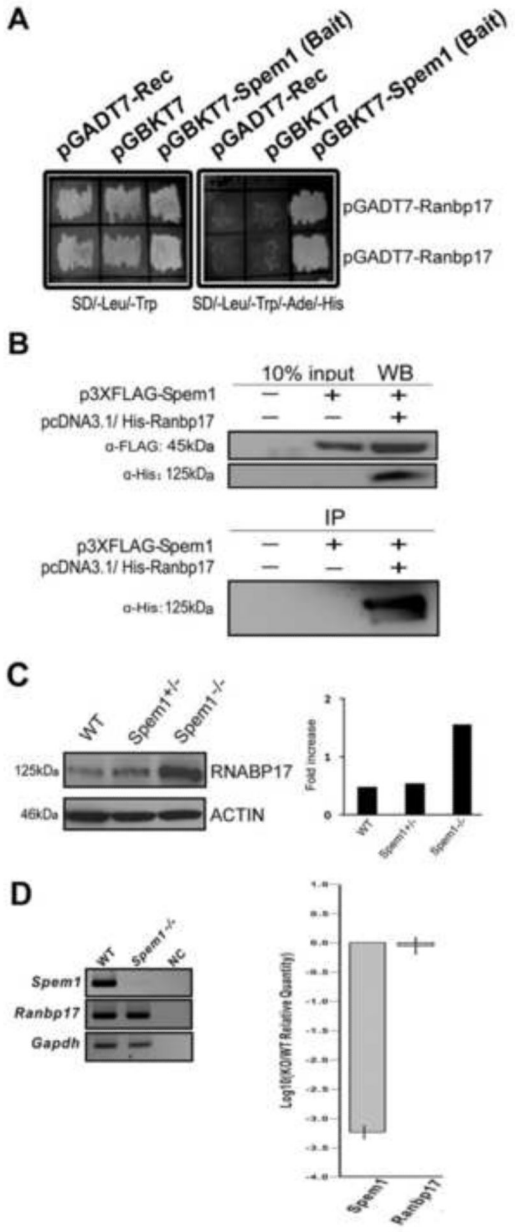

FIG. 1.

Identification of interactions between RANBP17 and SPEM1. **A**) Yeast co-transformation assays showing interactions between SPEM1 and two independent clones expressing RANBP17. On non-selective plates (SD/-Leu/-Trp) all transformed yeast cells grew, indicating viability of the cells and non-toxicity of the plasmids. Only cells co-transformed with pGBKT7-Spem1 and pGADT7-Ranbp17 grew on the selective plates (SD/-Leu/-Trp/-His/-Ade), demonstrating true interactions between RANBP17 and SPEM1 in yeast cells. **B**) Pull-down assays to verify the RANBP17-SPEM1 interactions in mammalian cells. FLAG-tagged SPEM1 and His-tagged RANBP17 were both expressed in the COS-7 cells, as shown by Western blot analyses (WB). In the immunoprecipitation (IP) assays, His-tagged RANBP17 was detected in the anti-FLAG immunoprecipitants, suggesting RANBP17 indeed interacts with SPEM1 in mammalian cells. **C**) RANBP17 levels were drastically elevated in *Spem1*$^{-/-}$ testes. The left panel shows a representative Western blot analysis of

RANBP17 levels in adult wild-type (WT), *Spem1*$^{+/-}$ and *Spem1*$^{-/-}$ testes. ACTIN was used as a loading control. Histograms to the right show quantitative analyses of the Western blot results on RANBP17 levels in WT, *Spem1*$^{+/-}$ and *Spem1*$^{-/-}$ testes. **D**) Levels of *Ranbp17* mRNA in wild-type (WT) and *Spem1*$^{-/-}$ testes. Representative results of semi-quantitative RT-PCR analyses on levels of *Ranbp17* mRNA in WT and *Spem1*$^{-/-}$ testes are shown in the left panel. NC, non-template control. Changes of *Ranbp17* mRNA levels in *Spem1* knockout (KO) testes relative to those in WT testes [Log_{10} (KO/WT levels)] are shown in the right panel. Mouse reference gene *Gapdh* was used as loading/internal control in both quantitative analyses.

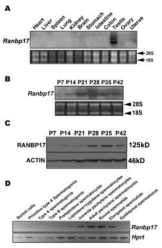

FIG. 2.

Expression of *Ranbp17* mRNA and protein in multiple mouse organs, developing testes, and purified testicular cell populations. **A**) Northern blot analyses of *Ranbp17* mRNA in 12 mouse organs. 28S and 18S rRNA bands were shown as loading and mRNA quality controls. **B**) Northern blot analyses of *Ranbp17* mRNA in developing testes in mice. Testes of postnatal days 7–42 (P7–P42) were analyzed, and 28S and 18S rRNA bands were shown as loading and mRNA quality controls. **C**) Western blot analyses of RANBP17 in mouse developing testes. ACTIN was used as a loading control. **D**) Levels of *Ranbp17* mRNA in purified testicular cell populations determined by semi-quantitative PCR analyses. Mouse reference gene hypoxanthine-guanine phosphoribosyltransferase (*Hprt*) was used as loading control. PCR cycle number for *Ranbp17* and *Hprt* were 25 and 20, respectively, which were tested to be within the exponential range.

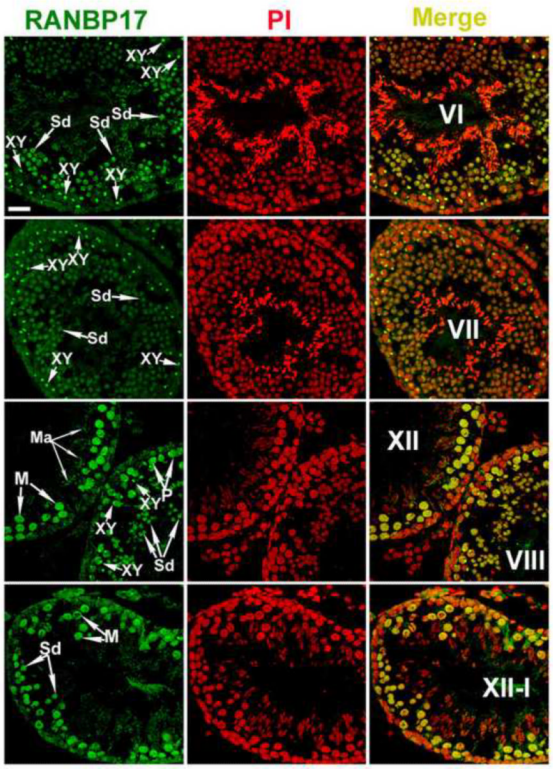

FIG. 3.

Immunofluorescent detection of RANBP17 in adult mouse testes. Green signals represent the immunoreactivity of RANBP17 and the cell nuclei were counter-stained with propidium iodide (PI). Stages of the seminiferous epithelial cycle are shown in Roman numerals. XY, the XY body; Sd, spermatid; M, meiotically dividing spermatocyte, P, pachytene spermatocyte; Ma, the manchette. All panels are in the same magnification. Scale bar = 20μm.

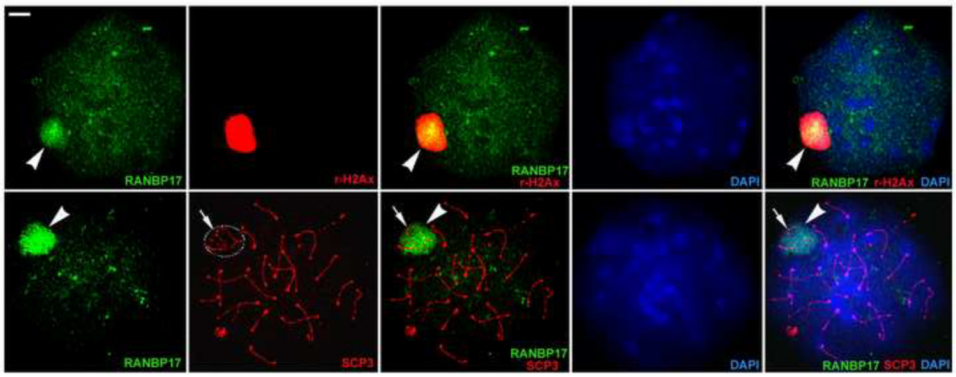

FIG. 4.

Immunofluroscent detection of RANBP17 in chromosome surface spreads of pachytene spermatocytes. In pachytene spermatocyte chromosome spreads, RANBP17 immunoreactivity (green and arrowheads) is predominantly concentrated in the XY body, which is strongly labeled by γH2Ax immunoreactivity (red in upper panels). Synaptonemal complexes of meiotic chromosomes are labeled as red fluorescence by the anti-SCP3 antibody and the XY body represents a sub-nuclear domain that can readily be distinguished based upon the shape of the SCP3-positive structures of the sex chromosomes (circle and arrows in lower panels). RANBP17 immunoreactivity is predominantly localized to the XY body. All panels are in the same magnification. Scale bar = 1μm.

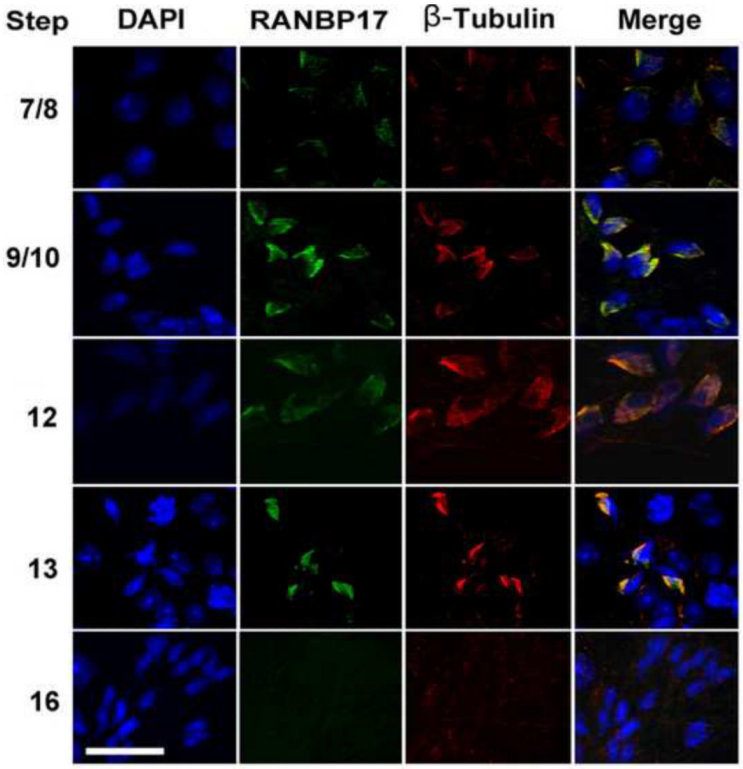

FIG. 5.

Immunofluorescent localization of RANBP17 to the manchette of wild-type elongating spermatids. Green fluorescence represents the RANBP17 immunoreactivity and red fluorescence indicates the immunoreactivity of β-Tubulin, a marker for the manchette. Cell nuclei were counterstained using DAPI (blue). Arabic numbers on the left indicate steps of the developing spermatids. All panels are in the same magnification. Scale bar = 20μm.

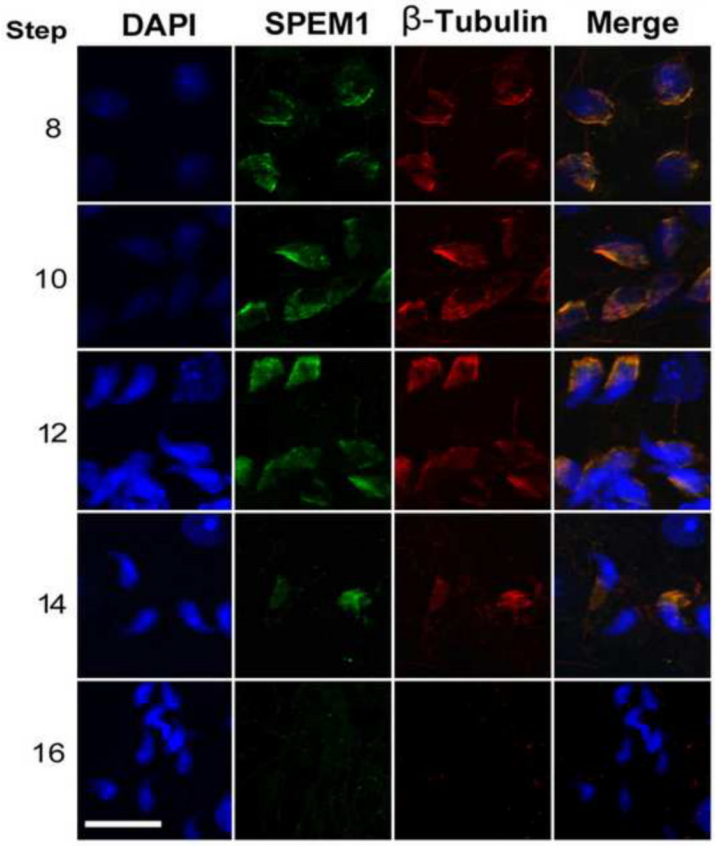

FIG. 6.

Immunofluorescent localization of SPEM1 to the manchette of wild-type elongating spermatids. Green fluorescence represents the SPEM1 immunoreactivity and red fluorescence reflects the immunoreactivity of β-Tubulin, a marker for the manchette. Cell nuclei were counterstained using DAPI (blue). Arabic numbers on the left stand for steps of the developing spermatids. All panels are in the same magnification. Scale bar = 20μm.